Journal of Beijing Institute of Technology, 2023, Vol. 32, No. 6

Modeling and Analysis of the Impacts of Temporal-Spatial Variant Troposphere on Ground-Based SAR Imaging of Asteroids

Tingting Fu, Yuanhao Li✉, Zhiyang Chen, Zheng Wu, Cheng Hu

Abstract: The near-Earth asteroid collisions could cause catastrophic disasters to humanity and the Earth, so it is crucial to monitor asteroids. Ground-based synthetic aperture radar (SAR) is an observation technique for high resolution imaging of asteroids. The ground-based SAR requires a long integration time to achieve a large synthetic aperture, and the echo signal will be seriously affected by temporal-spatial variant troposphere. Traditional spatiotemporal freezing tropospheric models are ineffective. To cope with this, this paper models and analyses the impacts of temporal-spatial variant troposphere on ground-based SAR imaging of asteroids. For the background troposphere, a temporal-spatial variant ray tracing method is proposed to trace the 4D (3D spatial + temporal) refractive index network provided by the numerical weather model, and calculate the error of the background troposphere. For the tropospheric turbulence, the Andrew power spectral model is used in conjunction with multiphase screen theory, and varying errors are obtained by tracking the changing position of the pierce point on the phase screen. Through simulation, the impact of temporal-spatial variant tropospheric errors on image quality is analyzed, and the simulation results show that the X-band echo signal is seriously affected by the troposphere and the echo signal must be compensated.

Keywords: near-Earth asteroids; ground-based SAR; troposphere; ray tracing

1 Introduction

The orbits of near-Earth asteroids are close to Earth's orbit, and there is a possibility of collision with the Earth, which poses a great threat to humanity. Coping with the risk of near-Earth asteroid impact is a major long-term challenge, so it is of great significance to monitor asteroids [1].

Ground-based radar is an effective technique for near-Earth asteroids observation. It actively emits electromagnetic waves and receives the reflection of asteroids. This allows for active observation throughout the day and in all weather conditions[2, 3].

Near-Earth asteroids are very far away and small in size, requiring high-resolution observation, which can be achieved by two technical approaches: one is to form a distributed radar with large diameter and high power by using multiple unit radars; the other is to mount a radar with a moving platform, such as a vehicle, to form a large synthetic aperture, which is ground-based synthetic aperture radar (SAR) [4]. The second technology has strong flexibility, low

Manuscript received Oct. 6, 2023; revised Oct. 21, 2023; accepted Nov. 27, 2023. The associate editor coordinating the review of this manuscript was Dr. Fengming Hu . This work was supported in part by the National Natural Science Foundation of China (Nos. 62101039, 62201051), in part by the Shandong Excellent Young Scientists Fund Program (Overseas), and in part by China Postdoctoral Science Foundation(No. 2022M720443).

Tingting Fu, Yuanhao Li, Zhiyang Chen and Cheng Hu are with Radar Research Laboratory, School of Information and Electronics, Beijing Institute of Technology, Beijing 100081, China.

Tingting Fu, Yuanhao Li, Zhiyang Chen and Cheng Hu are with Beijing Key Laboratory of Embedded Real-time Information Processing Technology.

Zheng Wu is with the Chongqing Institute of Meteorological Sciences, Chongqing 401147, China.

✉ Corresponding author. Email: lyh.900101@163.com

DOI: 10.15918/j.jbit1004-0579.2023.095

cost and easy implementation.

Compared with spaceborne SAR system, the platform of ground-based SAR system moves at a slower pace, so the integration time for obtaining high-resolution images is much longer, typically, several hours. Besides, ground-based SAR observes aerial targets, so the signal propagation path passes through a much wider area of the troposphere (hundreds of kilometres). The long integration time and synthetic aperture will cause spatial-temporal variant tropospheric impacts on asteroids imaging [5]. The troposphere is generally modeled into two parts: the background troposphere (slowly varying portion which introduces signal propagation delays[6]) and tropospheric turbulence (rapidly varying portion which causes random fluctuations in signal amplitude and phase [7]).

The tropospheric impacts on spaceborne SAR imaging have been widely studied [8]. The modeling methods of background troposphere are mainly based on traditional ray-tracing and mapping functions methods [9]. The ray-tracing methods are to calculate tropospheric delay through path integration of refractivity [10]. The mapping functions methods directly convert zenith delay into slant delay and are primarily used for high elevation angle conditions [11]. These methods are often combined with empirical tropospheric models, such as Hopfield model [12], Saastamoinen model [13], Egnos model [14], etc. For the tropospheric turbulence, statistical turbulence theory, i.e., turbulence power spectrum model, is primarily to model turbulence phase screens. Typical power spectrum models include the Kolmogorov spectrum [7], Tatarskii spectrum [15], Andrews spectrum [16]. The above models are generally combined with multi-phase screen theory to model amplitude phase errors caused by turbulence [17].

Since the integration time of spaceborne SAR is only a few minutes or less, and the signal path spans far less than a hundred kilometres in the troposphere in the horizonal direction, these studies are mainly based on the assumption of a spatiotemporal freezing model, i.e., the troposphere remains constant in time, and they only consider the change of the troposphere at different heights, neglecting horizontal tropospheric variations. Even in the research of geosynchronous (GEO) SAR systems with a long integration time up to 1 000 s, the tropospheric modeling is based on these two methods[18, 19]. The integration time of GEO SAR is much less than ground-based SAR, and the location of the pierce point in the troposphere is nearly unchanged. Therefore, the above modeling methods cannot simulate the temporal-spatial variant troposphere at the scale of ground-based SAR.

To solve the above problem, this paper proposes a method for modeling and analyzing the impact of temporal-spatial variant troposphere on ground-based SAR imaging of asteroids. For large-scale background troposphere, we propose the temporal-spatial variant ray tracing method to trace the 4D refractive index network calculated by numerical weather models (NWM) and estimate the propagation path delay accurately to obtain the error model. For small-scale tropospheric turbulence, use the Andrew power spectrum model in conjunction with the multi-phase screen theory to model the effects, according to the change in the position of the signal through the turbulent phase screen to obtain the varying errors. Finally, the influence of tropospheric effect is analysed theoretically and simulated.

The structure of this paper is as follows. In Section 2, we give the accurate signal model of ground-based SAR under the influence of troposphere. In Sections 3 and 4, the errors of background troposphere and tropospheric turbulence are modeled, respectively. In Section 5, the effect of troposphere on SAR imaging is simulated. Finally, conclusions are drawn in Section 6.

2 Ground-Based SAR Signal Model

Ground-based SAR can obtain an equivalent large aperture through the movement of the platform, enabling the long-range detection of asteroids. The integration time can reach a few hours, and the synthetic aperture trajectory spans over thousands of kilometres. The geometric structure diagram of ground-based SAR imaging is shown in Fig.1.

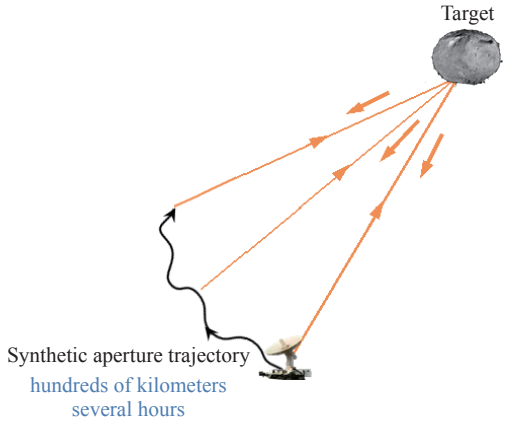

Fig. 1 Geometric structure of ground-based SAR imaging

Assuming $\boldsymbol{r}_{\mathrm{s}}(t_{\mathrm{a}})$ represents the position vector of the radar at time t_{a} and $\boldsymbol{r}_{\mathrm{r}}$ is the position vector of the target, the instantaneous slant range of the SAR signal at time t_{a} can be represented as

$$\begin{aligned} r(t_{\mathrm{a}}) = \| \boldsymbol{r}_{\mathrm{s}}(t_{\mathrm{a}}) - \boldsymbol{r}_{\mathrm{r}} \| \quad = \\ r_0 + q_1 t_{\mathrm{a}} + q_2 t_{\mathrm{a}}^2 + q_3 t_{\mathrm{a}}^3 \cdots \end{aligned} \tag{1}$$

where t_{a} is the slow time, r_0 is the slant range at the aperture center time, and q_i is the i-th order derivative with respect to slow time.

Considering the troposphere effects, the accurate echo signal of the ground-based SAR can be expressed as

$$\begin{aligned} s(t_{\mathrm{a}}, t) = & A_{\mathrm{r}}(t) A_{\mathrm{a}}(t_{\mathrm{a}}) \times \\ & \exp\left[\mathrm{j}\pi K_{\mathrm{r}} \left(t - \frac{2r(t_{\mathrm{a}})}{c} \right)^2 \right] \times \\ & \exp\left[-\mathrm{j}4\pi \frac{r(t_{\mathrm{a}})}{\lambda} \right] \times \\ & \exp\left\{ -\mathrm{j}\left(\Delta\varphi_{\mathrm{atmos}}(p, t_{\mathrm{a}}) \right) \right\} \end{aligned} \tag{2}$$

where t is the fast time, $A_{\mathrm{r}}(\cdot)$ and $A_{\mathrm{a}}(\cdot)$ are the envelope function in range and azimuth, respectively, K_{r} is the range frequency modulation rate, and λ is wavelength. And $\Delta\varphi_{\mathrm{atmos}}(p, t_{\mathrm{a}})$ is the total tropospheric phase error, and p is the different locations. At different moments and locations, the tropospheric conditions vary obviously. The temporal-spatial variant troposphere results in the varying degree of tropospheric impact on the signals of different synthetic aperture time. However, traditional empirical models cannot describe the temporal-spatial variant troposphere. Therefore, it is essential to combine 4D meteorological data provided by NWM to accurately estimate the tropospheric effects.

3 Modeling and Impacts Analysis of Background Troposphere

The core idea of the proposed method is to calculate refractivity based on 4D meteorological data provided by NWM, which can reflect temporal-spatial variant troposphere. Then the 4D grid of refractive index is tracked by the proposed algorithm called temporal-spatial variant ray tracing method to estimate the propagation path of the signal in the troposphere. The temporal-spatial variant error model can be obtained by the path integral of refractive index.

3.1 Refractive Index Calculation Using NWM

The impact of the troposphere on the propagation of electromagnetic waves can be typically represented by the refractive index N. The spatial and temporal distribution of the refractive index is related to the distribution of three meteorological factors: temperature T, water vapor pressure e, and tropospheric pressure P. The refractive index N is categorized into dry item N_{d} and wet item N_{w}. N can be expressed as

$$N = N_{\mathrm{d}} + N_{\mathrm{w}} = k_1 \frac{P_{\mathrm{d}}}{T} + \left(k_2 \frac{e}{T} + k_3 \frac{e}{T^2} \right) \tag{3}$$

where the atmospheric pressure of dry air is $P_{\mathrm{d}} = P - e(\mathrm{hPa})$, with T representing temperature in Kelvin (K). Thayer provides reference values for $k_1 = 77.604 \pm 0.014$, $k_2 = 64.79 \pm 0.08$, and

$k_3 = 377\,600 \pm 400$, respectively[20].

Using the High-precision ECMWF (European Centre for Medium-Range Weather Forecasts) ERA5 numerical weather model to model errors. The ERA5 model can provide meteorological parameters such as specific humidity, temperature, and pressure with a spatial resolution of 0.25°×0.25° at hourly intervals and a vertical resolution of 37 layers.

The value of water vapor pressure is difficult to measure and can be obtained from specific humidity q:

$$e = \frac{qP}{0.622 + 0.378q} \tag{4}$$

Because the ERA5 model is based on a geopotential height system, while the radar system is the geodetic height system. It is necessary to convert geopotential height to geodetic height. The method for converting the height system can be found in reference [21]. After standardizing the height system, tropospheric refractive index for each layer can be calculated using the meteorological para- meters for each layer.

3.2 Path Delay Calculation by Temporal-Spatial Variant Ray Tracing

The main idea of the temporal-spatial variant ray tracing method is to use a 4D refractive index network based on ERA5 model, estimating the signal's propagation path through the troposphere. The precise delay is obtained by the path integral of the refractive index. The specific steps of the proposed algorithm are as follows:

1) Step 1: Resample to obtain a 2D refractive index grid containing the signal propagation path.

Firstly, to calculate the refractive index in the troposphere and the heights of each layer based on the ERA5 model to obtain the temporal-spatial variant 4D refractive index network. Selecting the 3D refractive index network of the current synthetic aperture time, with the signal propagation path projected horizontally on the ground as the horizontal direction and zenith direction as the vertical direction. Then, resampling to obtain a two-dimensional refractive index grid containing the signal propagation path, where the grid cells are uniform in the horizontal direction, and the heights in the vertical direction are measured in terms of actual distances of the horizontal grid.

2) Step 2: Propagation path estimation.

Based on the angle of incidence θ and the coordinate of entry into this layer, determine whether the signal propagation path crosses the top boundary of the cell. The cell height is defined as the height difference Δh between adjacent layers provided by the ERA5 model. Due to the slow variation of the refractive index in the horizontal direction, the change in angles caused by refraction between the same altitude layers is not considered. The entry point into the current layer is denoted as $(x_{\text{in}}, y_{\text{in}})$, and the coordinates of exit from this layer are determined based on the incident angle $(x_{\text{out}}, y_{\text{out}})$, as shown in Fig2.

$$x_{\text{out}} = x_{\text{in}} + \tan\theta \times \Delta h \tag{5}$$

If x_{out} is greater than $\lceil x_{\text{out}} \rceil$ (the symbol $\lceil\rceil$ represents rounding up to the nearest integer.), it indicates that the signal did not cross the top of the cell. In this case, calculate the coordinates (x_n, y_n) of exiting this cell and proceed to calculate the next cell. Otherwise, x_{out} is less than $\lceil x_{\text{out}} \rceil$, it indicates a crossing, and the calculation for the next layer is performed.

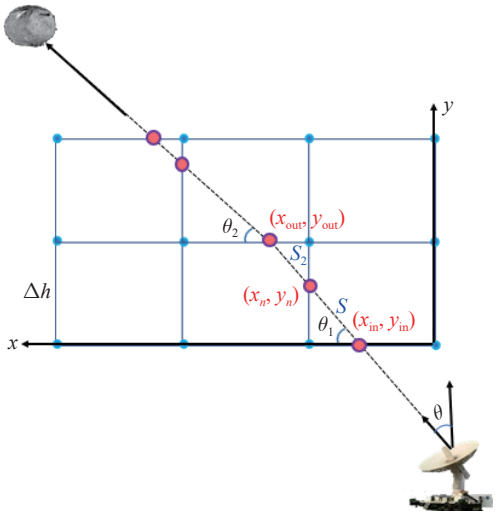

Fig. 2 Signal passing through refractive index grids

$$\begin{cases} x_n = x_{\text{in}} + 1 \\ y_n = y_{\text{in}} + \dfrac{\lceil x_{in} \rceil - x_{\text{in}}}{\tan\theta} \end{cases} \tag{6}$$

Calculate the slant range path Δs_i within the corresponding cell based on the coordinate of the entry point, to integrate and obtain the slant range delay, and to add it to the delay for this layer. To continue iterating until the ray reaches the top layer.

$$r = 10^{-6} \int N \times \mathrm{d}s = 10^{-6} \Sigma N_i \times \Delta s_i \tag{7}$$

3) Step 3: Update the angle of incidence.

Due to the troposphere causing the bending of signal propagation paths, changes in the angle of incidence require to be considered. Refractive index changes slowly in the horizontal direction, so only changes in angles between different height layers are considered, ignoring variations in angles when crossing different grids at the same height layer. Based on Snell's law, under the assumption of a spherical layered model, the product of refractive index at different heights, Earth's radius, and cosine of the elevation angle remains constant.

$$n_l(h_l + R)\cos\theta_l = n_{l+1}(h_{l+1} + R)\cos\theta_{l+1} \tag{8}$$

where n_l and θ_l represent the refractive index and angle of incidence when passing through the l-th layer of the grid. n_{l+1} and θ_{l+1} represent the refractive index and angle of incidence when entering the (l+1)-th layer of the grid. R is the Earth's radius.

4) Step 4: Calculate the delay from the model top to an altitude of 60 km.

The ERA5 model provides meteorological data up to approximately 47 km in altitude. However, above the top layer, there is minimal water vapor influence. The top tropospheric delay Δr_{top} from the top layer to 60 km is calculated using the Saastamoinen dry delay model, and the total delay Δr is finally obtained.

$$r_{\text{top}} = \cos\theta \times 0.002\,277 \times \frac{P}{f(\phi, h_{\text{top}})} \tag{9}$$

$$\Delta r = 10^{-6} \Sigma N_i \times \Delta s_i + r_{\text{top}} \tag{10}$$

where $f(\varphi, h)$ is the correction due to the Earth's rotation-induced gravitational acceleration, φ is the latitude, h is the height (kilometres).

$$f(\varphi, h) = 1 - 0.002\,66\cos 2\varphi - 0.000\,28h \tag{11}$$

5) Step 5: Iteratively compute delays for all synthetic aperture time.

Update the position of radar and repeat the steps from Step 1 to Step 4 to obtain the tropospheric delays corresponding to the entire synthetic aperture time.

6) Step 6: Modeling the temporal-spatial variant phase error.

Considering the bidirectional propagation of the SAR signal, the temporal-spatial variant phase error model is modeled based on the calculated time delay error $\Delta r\,(p, t_{\text{a}})$ can be expressed as

$$\begin{aligned} &\Delta\varphi_{\text{trop}}\,(p, t_{\text{a}}) = \frac{4\pi\Delta r\,(p, t_{\text{a}})}{\lambda} = \\ &\frac{4\pi}{\lambda}\left[q_1(p_1)t_{\text{a}} + q_2(p_2)t_{\text{a}}^2 + q_3(p_3)t_{\text{a}}^3 + \cdots\right] \end{aligned} \tag{12}$$

where t_{a} is the slow time, q_i is the i-th order derivative with respect to slow time, and p denotes the different locations.

The overall workflow of this algorithm is shown in Fig. 3.

The troposphere is a non-dispersive medium, and its impact on signals at different frequencies is consistent, which does not affect range imaging. Therefore, for ground-based SAR azimuth signals, phase error modeling takes the form of a series expansion that varies slowly with time. Considering the background tropospheric effects, the azimuth signal can be expressed as

$$\begin{aligned} s\,(t_{\text{a}}) =& \operatorname{rect}\left(\frac{t_{\text{a}}}{T_{\text{a}}}\right)\exp\left(\mathrm{j}\pi f_{\text{dr}} {t_{\text{a}}}^2\right) \times \\ & \exp(\Delta\varphi_{\text{trop}}\,(p, t_{\text{a}})) \\ =& \operatorname{rect}\left(\frac{ta}{T_{\text{a}}}\right)\exp\left(\mathrm{j}\pi f_{\text{dr}} {t_{\text{a}}}^2\right) \times \\ & \exp\left(-\mathrm{j}\frac{4\pi}{\lambda}\left(q_1(p_1)t_{\text{a}} + q_2(p_2){t_{\text{a}}}^2 + \right.\right. \\ & \left.\left. q_3(p_3){t_{\text{a}}}^3 + \cdots\right)\right) \end{aligned} \tag{13}$$

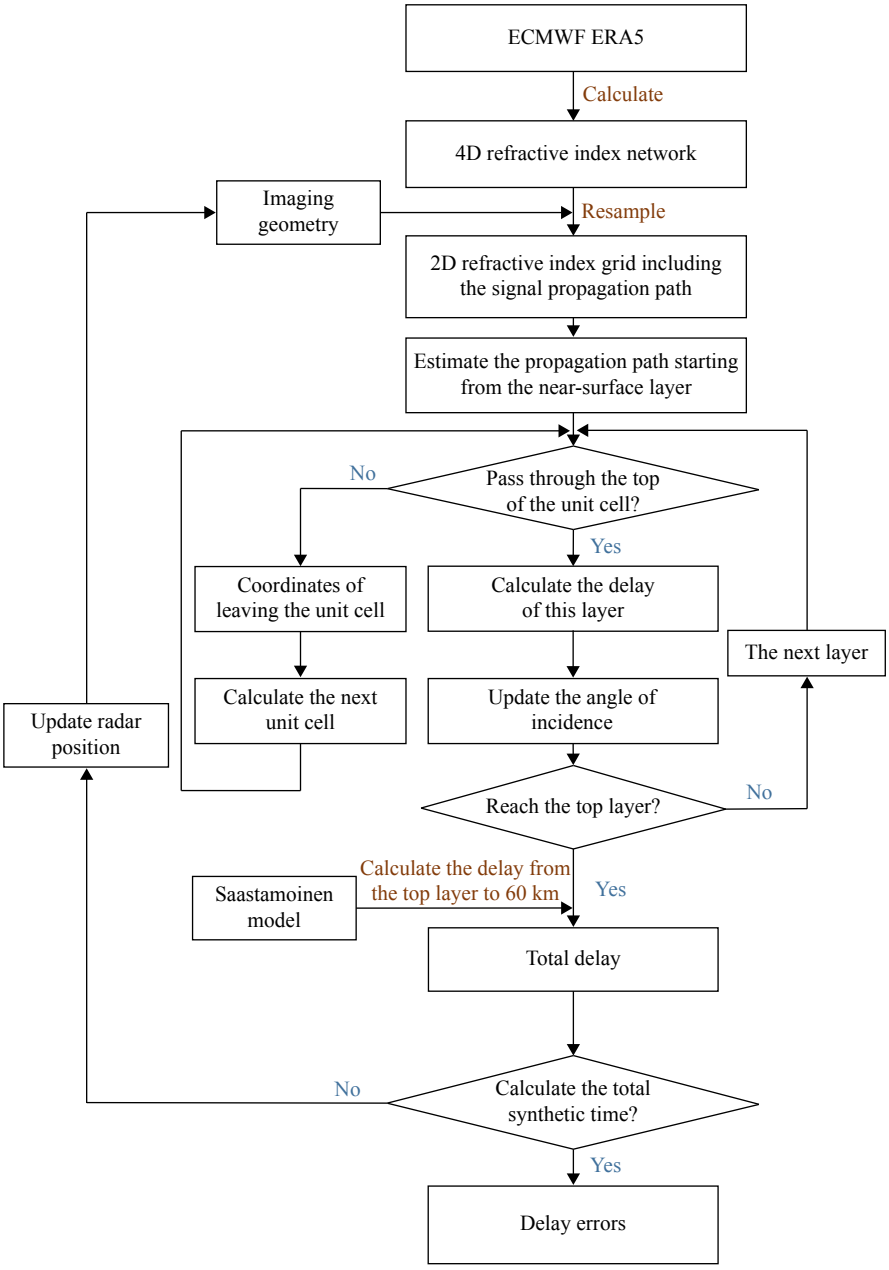

Fig. 3 Temporal-spatial variant ray tracing method flow chart

where T_a is the integration time, and f_{dr} is the azimuth frequency modulation rate.

The time rate of change of tropospheric delay affects the image quality, and the linearly changing part of the delay with time q_1 is related to the image offset.

$$\Delta L_a = v_{bf}\frac{2q_1}{\lambda f_{dr}} \tag{14}$$

where v_{bf} is the beam-foot velocity.

The nonlinear changing part q_2 causes quadratic phase error φ_{a2}, leading to the widening of the main lobe and the elevation of side lobes.

$$\varphi_{a2} = \frac{\pi q_2}{\lambda}T_a^2 \tag{15}$$

The nonlinear changing part q_3 leads to cubic phase error φ_{a3}, resulting in asymmetric side lobes and potentially causing azimuth defocusing [18].

$$\varphi_{a3} = \frac{\pi q_3}{2\lambda}T_a^3 \tag{16}$$

4 Modeling and Impacts Analysis of Tropospheric Turbulence

Tropospheric turbulence occurs due to irregular and random variations of meteorological parameters in both time and space, especially under certain sudden and extreme weather conditions. This leads to random fluctuations in signal amplitude and phase, making it challenging to accurately and comprehensively describe these variations using mathematical expressions. Therefore, statistical methods are employed to characterize the changes in meteorological parameters, as well as amplitude and phase fluctuations.

The refractive index power spectral density of tropospheric turbulence follows a power-law spectral distribution. Modeling using the Andrews power spectral model [16], which is capable of describing the power spectral distribution of turbulence in all wavenumber domains.

$$\begin{aligned}\Phi_{\mathrm{n}}(\kappa) &= 0.033 C_{\mathrm{n}}^{2}\left(\kappa^{2}+\kappa_{0}^{2}\right)^{-11/6}\exp\left(-\kappa^{2}/\kappa_{l}^{2}\right)\times \\ &\left[1+1.802\left(\kappa/\kappa_{l}\right)-0.254\left(\kappa/\kappa_{l}\right)^{7/6}\right]\end{aligned} \tag{17}$$

where $\kappa=\sqrt{\kappa_x^{\,2}+\kappa_y^{\,2}+\kappa_z^{\,2}}$is the spatial wave number; $\kappa_x=2\pi/x$, $\kappa_y=2\pi/y$, $\kappa_z=2\pi/z$, $\kappa_l=3.3/l_0$, $\kappa_0=2\pi/L_0$. L_0 is the outer scale of turbulence, ranging from the order of meters to hundreds of meters, and l_0 is the inner scale of turbulence, typically on the order of millimeters. C_{n}^2 is the refractive index structure constant of the turbulence, which is used to describe turbulence intensity. It depends on altitude, wind speed, and wet refractive index N_{wet}.

The power spectrum $\Phi_{\mathrm{s}}(\kappa)$ of the random phase introduced by tropospheric turbulence can be obtained from the refractive index power spectrum $\Phi_{\mathrm{n}}(\kappa)$:

$$\Phi_{\mathrm{s}}(\kappa)=2\pi k^{2}\int_{\Delta x}\Phi_{n}(\kappa)\mathrm{d}h \tag{18}$$

where $k=2\pi/\lambda$, and Δx is the thickness of each layer.

According to the change of the position of the signal passing through the phase screen during the integration time, to obtain the corresponding temporal-spatial variant turbulent phase errors. Considering that the time correlation of turbulence is only a few minutes, the time update threshold is set according to its correlation. When the integration time exceeds this threshold, the turbulence phase screen is regenerated.

Using the multi-phase screen theory to analyze the amplitude and phase fluctuations caused by tropospheric turbulence. Firstly, the power spectrum of random phase is used to construct a filter to filter the complex Gaussian random number sequence. And then the phase random fluctuation is obtained by inverse discrete Fourier transform:

$$\Delta\varphi_{\mathrm{turb}}=\frac{1}{N}\sum_{m=0}^{N-1}N\sqrt{\Phi_{\mathrm{s}}(m\Delta\kappa)\Delta\kappa/2\pi}\times r_{\mathrm{m}}\times\mathrm{e}^{2\pi inm/N} \tag{19}$$

where r_{m} is a Hermitian complex Gaussian random variable with zero mean and unit variance.

According to the multi-phase screen theory, the amplitude fluctuation I_{IF} and phase fluctuation φ_{TF} of the signal can be obtained by calculating the tropospheric transfer function D_{TF}.

$$\begin{aligned}D_{\mathrm{TF}}(u)=&I_{\mathrm{TF}}\exp(\mathrm{j}\phi_{\mathrm{TF}})= \\ &F^{-1}\left\{\exp\left[-\frac{\mathrm{j}\kappa^{2}}{2k}\Delta d\right]\left[F\left(\mathrm{e}^{\mathrm{j}\phi_{\mathrm{turb}}(u)}\right)\right]\right\}\end{aligned} \tag{20}$$

Due to the SAR signal bidirectional propagation, the tropospheric turbulence transfer function can be expressed as

$$D_{\mathrm{TF}}(u)=D_{\mathrm{TFup}}(u)\times D_{\mathrm{TFdown}}(u) \tag{21}$$

Turbulence will cause fluctuations in signal magnitude and phase, resulting in a degradation of the imaging quality of ground-based SAR. The azimuthal signal of SAR affected by tropospheric turbulence can be expressed as

$$\begin{aligned}s(t_{\mathrm{a}})=&\mathrm{rect}\left(\frac{t_{\mathrm{a}}}{T_{\mathrm{a}}}\right)\exp\left(\mathrm{j}\pi f_{\mathrm{dr}}t_{\mathrm{a}}^{2}\right)\times \\ &I_{\mathrm{IF}}(t_{\mathrm{a}})\exp(\mathrm{j}\varphi_{\mathrm{IF}}(t_{\mathrm{a}}))\end{aligned} \tag{22}$$

5 Simulations

5.1 Background Troposphere Effects Analysis

Simulation analysis of the background tropospheric impact on ground-based SAR azimuth imaging is conducted based on meteorological data provided by NWM. The temporal-spatial variant ray tracing method is employed in conjunction with high-precision ECMWF ERA-5 reanalysis model to simulate tropospheric delay errors.

Assuming the vehicle is the moving carrier of the radar and the Beijing-Shanghai Expressway as the synthetic aperture trajectory of ground-based SAR for simulation. The trajectory of the Beijing-Shanghai Expressway is shown in Fig.4. The trajectory length is approximately 1 220 km, and the time is about 12 hours. Selecting ERA5 data for 37 pressure levels, temperature, specific humidity, and surface geopotential from June 4th, 2023, 8:00 AM to 8:00 PM. The observed space target is a small celestial body located approximately 100 000 km away from Earth.

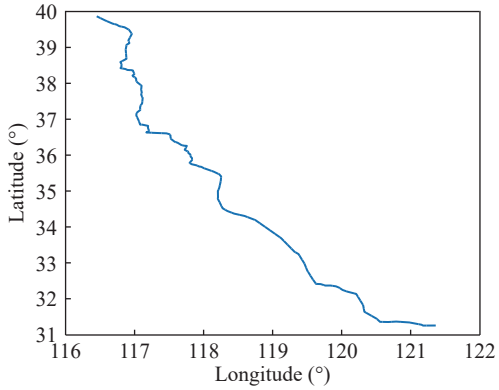

Fig. 4 Synthetic aperture trajectory

Using the temporal-spatial variant ray tracing method, to calculate the variation in tropospheric delay error within the synthetic aperture and compare it with the results calculated using the tropospheric empirical model called the Hopfield model [11]. The variation in delay error is shown in Fig.5, and the variation in phase error within the synthetic aperture time is obtained based on Eq.(12) and shown in Fig.6.

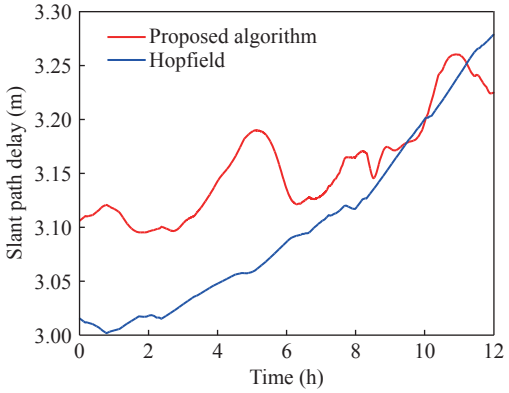

Fig. 5 Variation in tropospheric delay within the synthetic aperture time

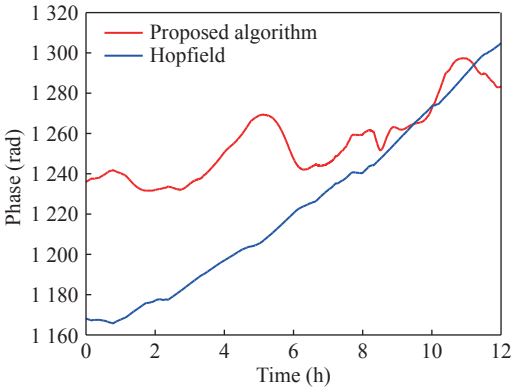

Fig. 6 Phase error corresponding to the X-band

From Fig.5 and Fig.6, it is evident that the time delay errors computed by both methods vary with synthetic aperture time. The proposed algorithm's delay ranges from a minimum of 3.09 m to a maximum of 3.26 m, while the delay calculated based on the Hopfield model ranges from 3 m to 3.27 m. The delay data calculated by the two methods are consistent, and the correlation coefficient is 86.74%. However, the Bias and RMSE reach 8.1 cm and 9.5 cm, respectively. The variations in delay obtained by the Hopfield model are primarily due to changes in the geometric structure of signal propagation, without accounting for the temporal-spatial variant atmospheric environment. Therefore, it can only provide a rough estimation of atmospheric delay and cannot describe its detailed variations. On the other hand, the numerical weather model, combined with spatiotemporal ray tracing considering the spatiotemporal characteristics of the tropospheric environment, enables precise calculation

of spatiotemporal variations in time delay errors during synthetic aperture time.

Based on the simulated imaging geometry, to assess the influence of troposphere on imaging results at different azimuthal resolutions. To achieve a specific azimuthal resolution, the required integration time is provided in Tab.1 calculating the corresponding peak sideLobe ratio (PSLR) and integral SsideLobe ratio (ISLR) to evaluate the imaging results, as shown in the Fig.7.

Tab. 1 The integration time required to achieve different resolutions

Azimuthal resolution (m)	Time (min)
1	615
2	290
3	200
5	118
10	54

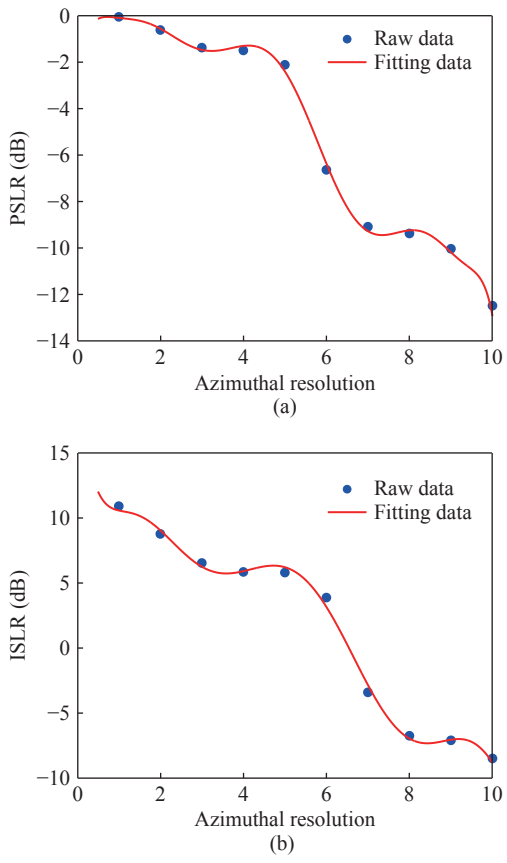

Fig. 7 Assessment of impacts on SAR imaging of troposphere at different resolutions: (a).PSLR; (b) LSLR

From Fig.7, it can be observed that the impact of the troposphere on SAR imaging varies with different resolution requirements. The higher the resolution requirement, the longer the integration time, and the more significant the influence of troposphere.

In the subsequent simulation analysis, the integration time is assumed to be 5 h for all cases. Adding the phase errors caused by background troposphere to the ground-based azimuthal echo signal as shown in Eq. (13), simulating and analysing the impact of temporal-spatial variant troposphere on ground-based SAR azimuthal imaging, obtaining the azimuthal profile as shown in Fig.8. Quantitatively analyse the impact of temporal rate of tropospheric delay variations on image quality, and calculate the PSLR and ISLR to obtain the imaging evaluation results shown in Tab.2.

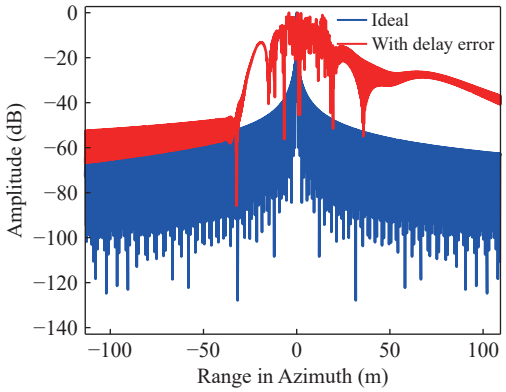

Fig. 8 The azimuthal profile

Tab. 2 Orbital elements

Parameter	Value
PSLR (dB)	-2.06
ISLR (dB)	6.73
Offset (m)	8144.2
Quadratic phase error (rad)	60.7
Cubic phase error (rad)	-123.97

According to SAR imaging theory, when the offset, second-order phase error, and third-order phase error are each smaller than one resolution cell, $\pi/4$ rad, and $\pi/8$ rad, respectively, their impact can be disregarded. Simulation results indicate that the linear variation of tropospheric delay results in significant offset in the SAR

image, while the nonlinear component leads to pronounced defocusing in SAR azimuthal imaging.

Therefore, the quality of ground-based SAR imaging is significantly degraded by temporal-spatial variant background tropos-phere.

5.2 Tropospheric Turbulence Effects Analysis

In the case of weak turbulence, the turbulence phase screen is simulated based on the Andrews power spectrum model, as shown in Fig.9.

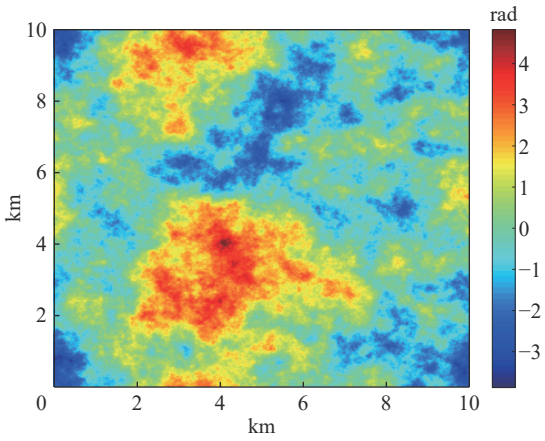

Fig. 9 Turbulence phase screen

Using the multiphase screen theory to simulate signal magnitude and phase variations caused by turbulence, assuming a time correlation of turbulence in the order of minutes, we assume that the turbulence phase screen remains unchanged within a 5-minute interval, and a new turbulence phase screen is generated every five minutes. During this period, only changes in position through the phase screen due to radar movement are considered. The signal magnitude and phase variations due to turbulence within the 5-minute interval are shown in Fig.10 and Fig.11, indicating random fluctuations in signal magnitude and phase.

Based on the Eq. (22) of the azimuthal signal model under the impact of turbulence in SAR signal, simulating the effect of tropospheric turbulence on azimuth imaging under the synthetic aperture time of 5h, the azimuth profile is obtained, as shown in Fig.12. The PSLR and ISLR are –13.64 dB and –1.78 dB, respectively. It can be observed that the azimuthal imaging result has defocusing obviously, so the effect of small-scale turbulence should also be considered.

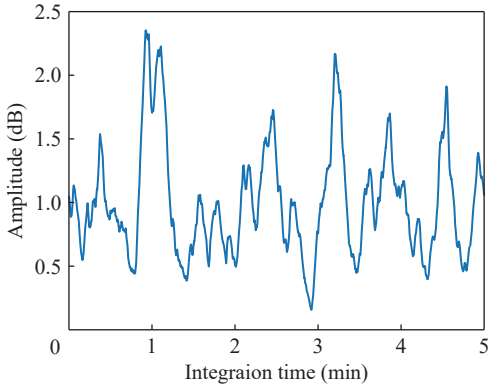

Fig. 10 Signal amplitude variation

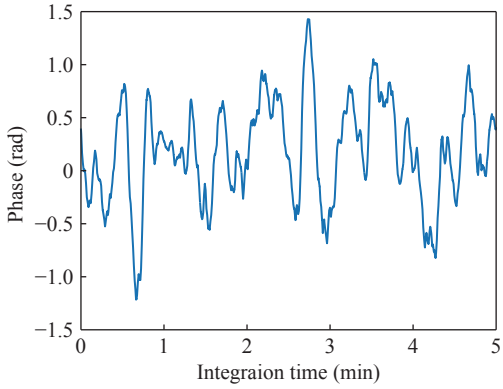

Fig. 11 Signal phase variation

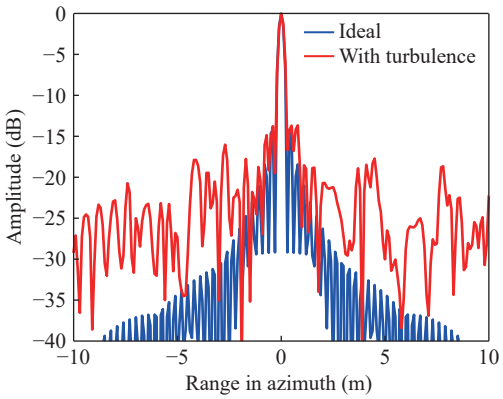

Fig. 12 Turbulence phase screen

5.3 Analysis of Two-Dimensional Imaging Effects on Point Targets

Combining the temporal-spatial variant errors of large-scale background tropospheric and small-scale tropospheric turbulence, an analysis of the two-dimensional imaging effects on point targets

is conducted based on the ground-based SAR signal model in Eq. (2). The result is shown in Fig.13.

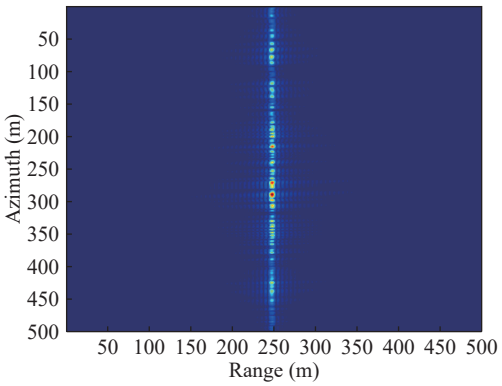

Fig. 13 Single point imaging

According to the imaging result, the azimuthal PSLR and ISLR are –1.29 dB and –0.81 dB, respectively. Simulation result shows that in the high-frequency X-band, temporal-spatial variant tropospheric errors can lead to severe defocusing in ground-based SAR azimuthal images. Therefore, to achieve high-resolution imaging in ground-based SAR, precise modeling and compensation of tropospheric errors are essential.

6 Conclusion

The prevention of asteroid impact is a major challenge for mankind. The ground-based SAR is an important technology for active observation of asteroids, and has a long integration time the synthetic aperture trajectory can span over a thousand kilometres. The temporal-spatial variant troposphere can lead to a degradation in the imaging performance of SAR, even causing defocusing. This paper models and analyses the troposphere at different scales. For slowly varying background troposphere, a high-precision numerical weather model is used in combination with temporal-spatial variant ray tracing for modeling. Tropospheric turbulence is modeled using a power-law spectral model combined with multi-phase screen theory. Then, analysing the impact of the temporal-spatial variant troposphere on ground-based SAR imaging based on the SAR echo signal model. Simulation results indicate that in the X-band, the SAR signal is significantly affected by the troposphere and requires compensation. Background troposphere causes azimuthal image offset and defocusing, while tropospheric turbulence leads to random phase error of the signal, thereby affecting azimuthal imaging.

References:

[1] S. Greenstreet, H. Ngo, and B. Gladman, "The orbital distribution of near-Earth objects inside Earth's orbit, " *Icarus,* vol. 217, no. 1, pp. 355-366, 2012.

[2] C. Jiong, W. Rui, and H. Cheng, "Maneuvering targets radar detection based on minimum entropy, " *Journal of Signal Processing,* vol. 338, no. 7, pp. 1416-1423, 2022.

[3] C. Jiong, W. Rui, and H. Cheng, "Target detection and density inversion of migrating insects based on a novel scanning insect radar, " *Journal of Signal Processing,* vol. 38, no. 7, pp. 1333-1352, 2022.

[4] X. Wu, H. Ma, and J. Zhang, "Development status and application of ground-based synthetic aperture radar, " *Journal of Wuhan University (Information Science),* vol. 44, no. 7, pp. 1073-1081, 2019.

[5] Z. Yu, Z. Li, and S. Wang, "An imaging compensation algorithm for correcting the impact of tropospheric delay on spaceborne high-resolution SAR, " *IEEE Transactions on Geoscience and Remote Sensing,* vol. 53, no. 9, pp. 4825-4836, 2015.

[6] Y. Li, P. L. Dekker, G. Mulder, L. Iannini, and P. Prats-Iraola, "Differential tropospheric delay estimation by simultaneous multi-angle repeat-pass InSAR, " *IEEE Transactions on Geoscience and Remote Sensing,* vol. 60, pp. 1-18, 2022.

[7] A. N. Kolmogorov, "Local structure of turbulence in an incompressible viscous fluid at very high reynolds numbers, " *Physics-Uspekhi,* vol. 10, no. 6, pp. 734-746, 1968.

[8] F. Zhang, G. Li, W. Li, and W. Hu, "Multiband microwave imaging analysis of ionosphere and troposphere refraction for spaceborne SAR, " *International Journal of Antennas and Propagation*, vol. 2014, pp. 1-9, 2014.

[9] D. Li, M. Rodriguez-Cassola, P. Prats-Iraola, "Modelling of tropospheric delays in geosynchronous synthetic aperture radar, " *Science in China Series F Information Sciences*, vol. 60, no. 6, pp. 1-18, 2017.

[10] L. Kou, M. Xiang, X. Wang, and M. Zhu, "Tropospheric effects on L-band geosynchronous circular SAR imaging, " *IET Radar, Sonar & Navigation*, vol. 7, no. 6, pp. 693-701, 2013.

[11] C. Qiu, X. Wang, Z. Li, S.Zhang, H. Li, J. Zhang, and H. Yuan , "The performance of different mapping functions and gradient models in the determination of slant tropospheric delay, " *Remote Sensing*, vol. 12, no. 1, pp. 130, 2020.

[12] S. Jinping, B. Yuekai, W. Yanping, and H. Wen, "High resolution SAR performance limitation by the change of tropospheric refractivity, " in *Proceedings of the 2011 IEEE CIE International Conference on Radar*, Chengdu, China, pp. 1498-1501,2011.

[13] A. Tuka and A. El-Mowafy, "Performance evaluation of different troposphere delay models and mapping functions, " *Measurement,* vol. 46, no. 2, pp. 928-937, 2013.

[14] H. Zhang, Y. Yuan, W. Li, Y. Li, and Y. Chai, "Assessment of three tropospheric delay models (IGGtrop, EGNOS and UNB3m) based on precise point positioning in the Chinese region, " *Sensors*, vol. 16, no. 1, pp. 122, 2016.

[15] V. I. Tatarski, *Wave propagation in a turbulent medium*, Courier Dover Publications, 1961.

[16] L. C. Andrews, "An analytical model for the refractive index power spectrum and its application to optical scintillations in the atmosphere, " *Journal of Modern Optics,* vol. 39, no. 9, pp. 1849-1853, 1992.

[17] A. M. Guarnieri, A. Leanza, A. Recchia, S. Tebaldini, and G. Venuti, "Atmospheric phase screen in GEO-SAR: estimation and compensation, " *IEEE Transactions on Geoscience and Remote Sensing*, vol. 56, no. 3, pp. 1668-1679, 2018.

[18] X. Dong, J. Hu, C. Hu, T. Long, Y. Li, and Y. Tian, "Modeling and quantitative analysis of tropospheric impact on inclined Geosynchronous SAR imaging, " *Remote Sensing*, vol. 11, no. 7, pp. 803, 2019.

[19] D. Li, M. Rodriguez-Cassola, P. Prats-Iraola, Z. Dong, M. Wu, and A. Moreira, "Modelling of tropospheric delays in geosynchronous synthetic aperture radar, " *Science China Information Sciences*, vol. 60, no. 6, pp. 060307, 2017.

[20] G. D. Thayer, "An improved equation for the radio refractive index of air, " *Radio Science*, vol. 9, no. 10, pp. 803-807, 1974.

[21] Z. Hu and J. J. Mallorquí, "An accurate method to correct atmospheric phase delay for insar with the era5 global atmospheric model, " *Remote Sensing,* vol. 11, no. 17, pp. 1969, 2019.

Tingting Fu received the B.S. degree in Electronic and Information Engineering from Hainan University, Hainan, China, in 2021. She is currently pursuing the Ph.D. degree in information and communication engineering with the Beijing Institute of Technology (BIT), Beijing, China. Her research interests include modeling and compensation technology of atmospheric impact on ground-based synthetic aperture radar (SAR) imaging.

Yuanhao Li received the B.S. degree in information engineering and the Ph.D. degree in Information and Communication Engineering from Beijing Institute of Technology (BIT), Beijing, China, in 2012 and 2018, respectively. He is currently an Associate Professor with the School of Information and Electronics, BIT, Beijing, China. His research interests include radar system design and signal processing, InSAR/D-InSAR technique, and radar altimeters constellations.

Zhiyang Chen received the B.S. degree and the Ph.D. degree from the Department of Electronic Engineering, Tsinghua University, Beijing, China, in 2016, and from the School of Information and Electronics (SIE), Beijing Institute of Technology (BIT), in 2021, respectively. He is now a Post-Doctoral Researcher in SIE, BIT. His research interests include geosynchronous synthetic aperture radar (GEO SAR) satellites formation design, SAR interferometry and SAR tomography.

Zheng Wu received the Ph.D. degree in atmospheric science from Nanjing University, Nanjing, China, in 2013, He is currently a senior engineering with the Chongqing Institute of Meteorological Sciences, Chongqing 401147, China. His research interests include radar data assimilation, meso-scale and small-scale numerical weather prediction in south-west China.

Cheng Hu (Senior Member, IEEE) received the B.S. degree in electronic engineering from National University of Defense Technology, Changsha, China, in 2003, and the Ph.D. degree in target detection and recognition from Beijing Institute of Technology (BIT), Beijing, China, in 2009. Since September 2009, he has been with School of Information and Electronics, BIT, and promoted to be a Full Professor in 2014, a Doctoral Supervisor, and Vice-Director of Radar Research Lab. His main research interests include new concept synthetic aperture radar imaging and the biological detection radar system and signal processing.